

CHIMERA-BENCH: A BENCHMARK DATASET FOR EPITOPE-SPECIFIC ANTIBODY DESIGN

Mansoor Ahmed^{1,2*}, Nadeem Taj³, Imdad Ullah Khan⁴, Hemanth Venkateswara¹,
Murray Patterson^{1*}

¹Georgia State University, Atlanta, GA, USA

²Georgia Institute of Technology, Atlanta, GA, USA

³University of Engineering and Technology, Lahore, Pakistan

⁴Lahore University of Management Sciences, Pakistan

ABSTRACT

Computational antibody design has seen rapid methodological progress, with dozens of deep generative methods proposed in the past three years, yet the field lacks a standardized benchmark for fair comparison and model development. These methods are evaluated on different SAbDab snapshots, non-overlapping test sets, and incompatible metrics, and the literature fragments the design problem into numerous sub-tasks with no common definition. We introduce CHIMERA-BENCH (CDR Modeling with Epitope-guided Redesign), a unified benchmark built around a single canonical task: *epitope-conditioned CDR sequence–structure co-design*. CHIMERA-BENCH provides (1) a curated, deduplicated dataset of **2,922** antibody–antigen complexes with epitope and paratope annotations; (2) three biologically motivated splits testing generalization to unseen epitopes, unseen antigen folds, and prospective temporal targets; and (3) a comprehensive evaluation protocol with five metric groups including novel epitope-specificity measures. We benchmark representative methods spanning different generative paradigms and report results across all splits. CHIMERA-BENCH is the largest dataset of its kind for the antibody design problem, allowing the community to develop and test novel methods and evaluate their generalizability. The source code and data are available at: <https://github.com/mansoor181/chimera-bench.git>

1 INTRODUCTION

Antibodies are among the most important classes of biotherapeutics (Norman et al., 2020). Their binding specificity is largely determined by six complementarity-determining regions (CDRs), particularly CDR-H3, which makes these loops the primary targets for computational design. Deep generative models have recently transformed this space, with diffusion models (Luo et al., 2022; Martinkus et al., 2023), flow matching (Tan et al., 2025), equivariant graph neural networks (Wu et al., 2025; Kong et al., 2022; 2023), autoregressive models (Jin et al., 2021), and foundation models (Wang et al., 2025) all proposed for CDR sequence–structure co-design. Yet despite this rapid progress, there is no standardized way to compare these methods. They are trained on different snapshots of the Structural Antibody Database (SAbDab) (Dunbar et al., 2014) with varying filtering criteria, evaluated on non-overlapping test sets from the RAbD dataset (Adolf-Bryfogle et al., 2018) to hold-outs, and scored with incompatible metrics computed under different definitions. For example, contact cutoffs vary from 4.5 to 6.6 Å across methods, and RMSD is computed with or without Kabsch alignment. The methods also require inputs in different and incompatible formats, making head-to-head comparison impractical without building separate data pipelines for each method.

A more fundamental issue is the absence of a common task definition. The literature fragments antibody design into numerous sub-tasks, including inverse folding, structure prediction, co-design, docking, affinity optimization, de novo generation, and epitope-conditioned design, and individual

*Address correspondence to: mahmed76@student.gsu.edu, mpatterson30@gsu.edu

methods address different subsets. This makes it unclear what is being compared, even when two papers report the same metric name. We argue that in many therapeutic settings, the target epitope is specified and propose *epitope-conditioned CDR sequence–structure co-design* as the canonical formulation. Given an antigen structure, an epitope specification, and an antibody framework, the task is to design CDR residues that are structurally valid, contact the target epitope, and avoid off-target binding. This formulation subsumes the sub-tasks above as special cases and accommodates all baseline methods. Methods that natively support epitope conditioning map directly to this definition, while the remaining methods can be evaluated as-is, with epitope-specificity metrics revealing whether their designs contact the intended site.

We introduce CHIMERA-BENCH (CDR Modeling with Epitope-guided Redesign), a benchmark dataset for this task. Our contributions are:

- A **canonical problem definition** that unifies seven sub-tasks from the literature into a single epitope-conditioned CDR co-design formulation.
- A **curated dataset** of deduplicated, quality-filtered antibody–antigen complexes from SAbDab, CDR masks, epitope/paratope annotations, and contact maps.
- **Three evaluation splits** (epitope-group, antigen-fold, and temporal), each with cluster-level leakage prevention, testing generalization along distinct biological axes.
- A **comprehensive evaluation protocol** with five metric groups covering sequence quality, structural accuracy, binding interface quality, epitope specificity, and designability, including novel epitope-specificity metrics not reported by any existing method.

2 RELATED WORK

Antibody CDR design methods. Early learning-based approaches to CDR design were autoregressive. RefineGNN (Jin et al., 2021) generates CDR residues left-to-right while iteratively refining the predicted structure, and AbDockGen (Jin et al., 2022) combines hierarchical equivariant refinement with antibody–antigen docking. MEAN (Kong et al., 2022) recast the problem as E(3)-equivariant graph translation, and dyMEAN (Kong et al., 2023) extended this to end-to-end full-atom antibody design. RAAD (Wu et al., 2025) later introduced relation-aware equivariance for settings where the epitope is unknown. Diffusion models have since become the dominant paradigm, beginning with DiffAb (Luo et al., 2022), which pioneered antigen-conditioned CDR diffusion over sequences, coordinates, and orientations simultaneously. AbX (Zhu et al., 2024) augmented this framework with evolutionary and physical constraints, and LEAD (Yao et al., 2025) introduced property-guided sampling through black-box optimization in a shared latent space. dyAb (Tan et al., 2025) applies flow matching to flexible antibody design using AlphaFold-predicted pre-binding antigen conformations, and AbODE (Verma et al., 2023) formulates CDR generation through conjoined ODEs. RFAntibody (Bennett et al., 2025) fine-tunes RFdiffusion on $\sim 8,100$ PDB antibody structures for de novo design of complete variable regions (VHHs and scFvs) conditioned on a target epitope. In the broader protein design space, BoltzGen (Stark et al., 2025) is an all-atom diffusion model that unifies binder design and structure prediction across modalities, including nanobodies, though it targets general binder design rather than CDR-level co-design. ProteinMPNN (Dauparas et al., 2022), while also not antibody-specific, serves as a strong inverse folding baseline for CDR sequence design given a fixed backbone.

Existing benchmarks and datasets. SAbDab (Dunbar et al., 2014) is the primary structural database for antibodies but provides no standardized splits, evaluation protocol, or task definition for generative design and contains redundant complexes that require preprocessing for training neural networks. The RAbD benchmark (Adolf-Bryfogle et al., 2018) defines 60 antibody–antigen complexes for CDR-H3 redesign but lacks epitope annotations and modern generative metrics such as DockQ or diversity. SKEMPI v2 (Jankauskaitė et al., 2019) provides experimental binding affinity measurements for protein complexes including approximately 53 antibody entries, but targets mutation-level affinity prediction rather than generative design. AbBiBench (Zhao et al., 2025) benchmarks antibody binding affinity maturation with 184,500+ experimental measurements across 14 antibodies, but focuses on affinity prediction rather than generative CDR design. In the broader protein domain, ProteinGym (Notin et al., 2023) benchmarks fitness prediction across 250+ deep mutational scanning assays and ATOM3D (Townshend et al., 2020) defines molecular learning tasks

on 3D structures, but neither addresses the antibody-specific challenges of CDR co-design, epitope conditioning, or binding interface evaluation. To our knowledge, CHIMERA-BENCH is the first benchmark to combine standardized data curation, biologically motivated splits, epitope-specificity metrics, and cross-method format compatibility for computational antibody design.

3 THE CHIMERA-BENCH BENCHMARK

3.1 TASK DEFINITION

As discussed above, the antibody design literature fragments the problem into numerous sub-tasks, and individual methods address different subsets. CHIMERA-BENCH consolidates these into a single canonical task, *epitope-conditioned CDR sequence–structure co-design*, motivated by the observation that in many therapeutic settings the target epitope is specified. Given an antigen structure $A = \{(s_j, \mathbf{x}_j) \mid j \in V_A\}$, an epitope $E \subseteq V_A$, and an antibody framework $F = \{(s_i, \mathbf{x}_i) \mid i \in V_{FR}\}$, the task is to design CDR residues that maximize the learned conditional distribution while satisfying epitope contact and precision constraints. Following Luo et al. (2022), each residue is represented as a tuple of amino acid type, $C\alpha$ coordinate, and local frame orientation. The remaining sub-tasks from the literature are subsumed as special cases: inverse folding fixes the backbone and designs sequence only (the ProteinMPNN setting), structure prediction fixes the sequence, unconditional co-design sets $E = V_A$ (i.e., the entire antigen surface is treated as the target, imposing no epitope constraint), and docking quality is captured implicitly through DockQ and iRMSD.

The task can be expressed concisely as:

$$R^* = \arg \max_R p_\theta(R \mid A, E, F), \quad \text{s.t. } \mathcal{C}(R, A) \cap E \neq \emptyset, \quad \mathcal{C}(R, A) \subseteq E \quad (1)$$

where $R = \{(s_k, \mathbf{x}_k, \mathbf{O}_k)\}_{k \in V_{\text{CDR}}}$ denotes the designed CDR residues with amino acid type s_k , $C\alpha$ coordinate \mathbf{x}_k , and local frame orientation \mathbf{O}_k , and $\mathcal{C}(R, A) = \{j \in V_A \mid \exists k \in V_{\text{CDR}} : \|\mathbf{x}_k - \mathbf{x}_j\| < d_c\}$ is the set of antigen residues contacted by the designed CDRs within a cutoff distance d_c .

3.2 DATASET CONSTRUCTION

The CHIMERA-BENCH dataset is constructed from SAbDab (Dunbar et al., 2014) through an eight-step pipeline (Figure 1). Starting from 20,509 SAbDab entries, we apply quality filters (protein/peptide antigens only, paired VH/VL chains, resolution $\leq 4.0 \text{ \AA}$), cluster at 95% sequence identity using MMseqs2 (Steinegger & Söding, 2017), and validate each complex for ANARCI (Dunbar & Deane, 2016) numberability, conserved residue presence, CDR completeness, and backbone integrity. Residues are numbered under both the IMG1 (Lefranc et al., 2003) and Chothia (Chothia & Lesk, 1987) schemes, and epitope/paratope residues are identified at a 4.5 \AA contact cutoff. The full processing details, validation criteria, and exclusion breakdown are provided in Appendix A.1.

The final dataset contains **2,922 complexes** from 2,721 unique PDBs (2,485 protein-antigen, 437 peptide-antigen, median resolution 2.72 \AA), with on average 17.9 epitope and 20.5 paratope residues per complex. Dataset statistics are in Appendix A.3 and graph construction details in Appendix A.9.

3.3 DATA SPLITS

A central design choice in CHIMERA-BENCH is the use of three biologically motivated splits, each testing a different generalization axis while enforcing cluster-level separation to prevent data leakage. The **epitope-group** split clusters complexes that share the same set of epitope residue positions on the antigen surface, so that the test set contains epitope patterns never seen during training. Two complexes belong to the same cluster if and only if their sorted epitope residue identifiers (chain, position) are identical, which naturally handles discontinuous epitopes. The **antigen-fold** split groups complexes by antigen identity, ensuring the test set contains entirely unseen antigen targets. The **temporal** split assigns complexes by PDB deposition date, simulating prospective deployment on structures deposited after the training period. Split sizes are in Table 4 (Appendix A.3).

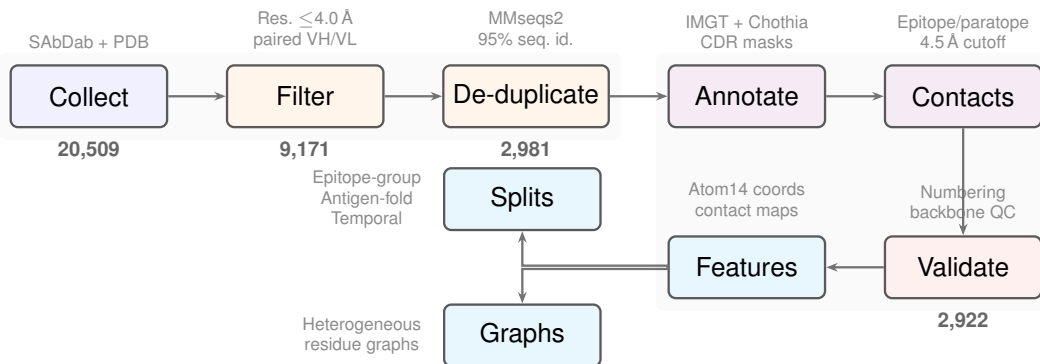


Figure 1: The CHIMERA-BENCH data curation pipeline that collects antigen-antibody complexes from SAbDab and produces filtered and annotated complexes for the antibody design task.

3.4 EVALUATION PROTOCOL

We evaluate designs across five metric groups that collectively assess sequence quality, structural accuracy, binding interface quality, epitope specificity, and designability. **Sequence quality** is measured by amino acid recovery (AAR) and contact AAR (CAAR), which restricts this calculation to paratope residues within 4.5 \AA of the antigen, along with perplexity (PPL) for models that produce sequence likelihoods. **Structural quality** is assessed by $C\alpha$ RMSD after Kabsch alignment and TM-score (Zhang & Skolnick, 2004). We standardize on Kabsch-aligned RMSD throughout, as existing methods use inconsistent implementations. The **binding interface quality** is captured by the fraction of native contacts recovered (Fnat), interface RMSD (iRMSD) restricted to contact residues, and the DockQ composite score (Basu & Wallner, 2016), which combines Fnat, iRMSD, and ligand RMSD into a single metric. **Epitope specificity** is a novel evaluation axis introduced by CHIMERA-BENCH. We compute epitope precision, recall, and F1, measuring whether a design contacts the intended binding site. **Designability** counts known sequence liability motifs associated with manufacturing issues. The formal definitions are provided in Appendix A.2.

4 EXPERIMENTS

We benchmark eleven antibody design methods spanning six generative paradigms (Appendix A.11): equivariant GNNs (RAAD, MEAN, dyMEAN), diffusion models and their extensions (DiffAb, AbMEGD, RADAb, AbFlowNet), flow matching (dyAb), autoregressive generation (RefineGNN), hierarchical equivariant networks (AbDockGen), and conjoined ODEs (AbODE). Each method is retrained on CHIMERA-BENCH using the authors’ released code with default hyperparameters. The training details are in Appendix A.6.

4.1 CDR-H3 DESIGN RESULTS

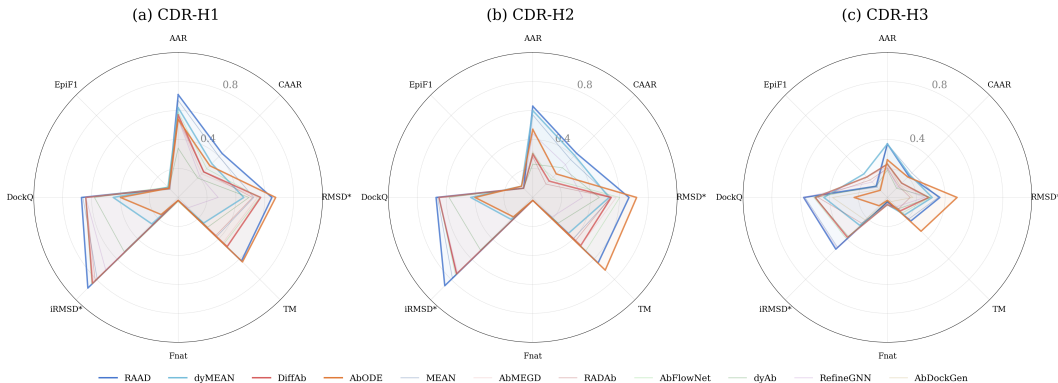
Table 1 reports CDR-H3 co-design results on the epitope-group test split, our primary evaluation setting. The results on the antigen-fold and temporal splits are provided in Tables 9 and 10 (Appendix A.11). All values are computed using the standardized CHIMERA-BENCH evaluation pipeline with Kabsch-aligned RMSD and a 4.5 \AA contact cutoff. Perplexity is reported as “–” for diffusion and flow-based models that do not produce sequence likelihoods.

4.2 ANALYSIS

Paradigm comparison. Figure 2 provides a visual summary across all eight core metrics for CDR-H1, H2, and H3. Equivariant GNN methods (RAAD, MEAN, dyMEAN) dominate sequence recovery, with AAR ~ 0.37 on the epitope-group split, while the diffusion-based methods (DiffAb, AbMEGD, RADAb, AbFlowNet) and the flow matching method dyAb cluster together at AAR ~ 0.19 – 0.23 . AbDockGen produces the worst structural quality (RMSD=4.67), while AbODE

Table 1: CDR-H3 design results of the baseline methods on the **epitope-group** test split. Best values are in **bold**, second-best are underlined. “-” indicates the metric is not applicable.

Method	AAR \uparrow	CAAR \uparrow	PPL \downarrow	RMSD \downarrow	TM \uparrow	Fnat \uparrow	iRMSD \downarrow	DockQ \uparrow	EpiF1 \uparrow	n_liab \downarrow
RAAD (Wu et al., 2025)	0.37\pm0.12	0.21 \pm 0.22	3.27 \pm 0.48	1.75 \pm 0.77	0.23 \pm 0.12	0.03 \pm 0.04	0.98\pm0.55	0.58\pm0.07	0.11 \pm 0.13	0.57 \pm 0.65
MEAN (Kong et al., 2022)	0.37\pm0.13	0.24\pm0.23	3.10\pm0.47	1.84 \pm 0.75	0.21 \pm 0.10	0.03 \pm 0.04	1.05 \pm 0.60	0.57 \pm 0.07	0.10 \pm 0.13	0.58 \pm 0.49
dyMEAN (Kong et al., 2023)	0.37\pm0.13	0.22 \pm 0.23	3.29 \pm 0.40	2.22 \pm 0.97	0.17 \pm 0.11	0.05\pm0.09	2.68 \pm 1.37	0.44 \pm 0.08	0.23\pm0.21	0.83 \pm 0.38
DiffAb (Luo et al., 2022)	0.23 \pm 0.12	0.14 \pm 0.19	-	2.49 \pm 1.28	0.13 \pm 0.10	0.05\pm0.06	1.56 \pm 0.79	0.50 \pm 0.12	0.20 \pm 0.18	0.52 \pm 0.71
AbFlowNet (Abir et al., 2025)	0.23 \pm 0.11	0.14 \pm 0.18	-	2.38 \pm 1.22	0.15 \pm 0.11	0.05\pm0.06	1.49 \pm 0.79	0.51 \pm 0.13	0.20 \pm 0.17	0.38 \pm 0.63
AbMEGD (Chen et al., 2025)	0.21 \pm 0.12	0.12 \pm 0.16	-	2.44 \pm 1.29	0.13 \pm 0.10	0.05\pm0.05	1.57 \pm 0.82	0.50 \pm 0.12	0.20 \pm 0.18	0.49 \pm 0.67
RADAb (Wang et al., 2024)	0.20 \pm 0.12	0.11 \pm 0.17	-	5.33 \pm 17.22	0.11 \pm 0.10	0.04 \pm 0.05	2.98 \pm 10.37	0.48 \pm 0.14	0.17 \pm 0.15	0.56 \pm 0.74
dyAb (Tan et al., 2025)	0.19 \pm 0.08	0.09 \pm 0.14	-	2.34 \pm 0.87	0.11 \pm 0.07	0.03 \pm 0.04	1.62 \pm 0.66	0.50 \pm 0.06	0.11 \pm 0.15	0.00\pm0.00
RefineGNN (Jin et al., 2021)	0.21 \pm 0.11	0.10 \pm 0.14	8.46 \pm 3.28	2.86 \pm 0.87	0.09 \pm 0.06	0.04 \pm 0.05	1.02 \pm 0.57	0.58\pm0.06	0.15 \pm 0.15	0.71 \pm 0.80
AbDockGen (Jin et al., 2022)	0.24 \pm 0.12	0.12 \pm 0.18	8.04 \pm 2.65	4.67 \pm 1.32	0.04 \pm 0.02	0.02 \pm 0.03	3.56 \pm 1.82	0.38 \pm 0.09	0.08 \pm 0.10	0.70 \pm 0.79
AbODE (Verma et al., 2023)	0.26 \pm 0.12	0.20 \pm 0.22	11.70 \pm 4.34	1.07\pm0.38	0.33\pm0.13	0.02 \pm 0.03	11.35 \pm 5.61	0.23 \pm 0.08	0.07 \pm 0.12	1.50 \pm 1.90

Figure 2: Radar plots comparing methods across metrics for CDR-H1, H2, and H3 on the epitope-group split. Six metrics (AAR, CAAR, TM, Fnat, DockQ, EpiF1) are shown on their native $[0, 1]$ scale; RMSD and iRMSD are transformed via $1/(1+x)$ so that higher values indicate better performance on all axes.

achieves paradoxically low CDR RMSD (1.07) but catastrophic interface placement (iRMSD=11.35, DockQ=0.23), indicating that its CDR loops are locally well-formed but positioned far from the binding interface. Among the equivariant GNNs, dyMEAN achieves the best epitope specificity (EpiF1=0.23) and highest Fnat (0.05), suggesting that its explicit interface modeling provides meaningful binding signal. All methods recover few native contacts (Fnat \sim 0.02–0.05), yet DockQ remains moderate (0.44–0.58) because single-CDR redesign preserves the overall interface geometry.

Epitope conditioning and generalization. The epitope-specificity metrics reveal a striking pattern: diffusion-based methods (DiffAb, AbFlowNet, AbMEGD) achieve higher EpiF1 (\sim 0.20) than sequence-dominant methods RAAD and MEAN (\sim 0.10–0.11), despite lower sequence recovery. dyMEAN bridges both capabilities with strong AAR (0.37) and the best EpiF1 (0.23). Across splits, most methods are stable, though MEAN’s EpiF1 drops from 0.10 on the epitope-group split to 0.09 on the temporal split, and AbODE’s already poor interface metrics degrade further on temporal targets (DockQ from 0.23 to 0.21). These findings validate both the multi-split design and the epitope-specificity metrics introduced by CHIMERA-BENCH.

5 CONCLUSION

We have presented CHIMERA-BENCH, a unified benchmark for epitope-specific antibody CDR design. CHIMERA-BENCH provides a canonical task formulation, a curated dataset of 2,922 complexes with three biologically motivated splits, and a standardized evaluation protocol with five metric groups, including novel epitope-specificity measures. Our evaluation of eleven baseline methods spanning different generative paradigms establishes comparisons under consistent conditions and reveals failure modes invisible under a single random split, such as the disconnect between local CDR quality and interface placement.

REFERENCES

- Abrar Rahman Abir, Haz Sameen Shahgir, Md Rownok Zahan Ratul, Md Toki Tahmid, Greg Ver Steeg, and Yue Dong. Abflownet: Optimizing antibody-antigen binding energy via diffusion-gflownet fusion. *arXiv preprint arXiv:2505.12358*, 2025. [5](#), [14](#), [15](#), [18](#)
- Jared Adolf-Bryfogle, Oleks Kalyuzhnyi, Michael Kubitz, Brian D Weitzner, Xiaozhen Hu, Yumiko Adachi, William R Schief, and Roland L Dunbrack Jr. Rosettaantibodydesign (rabd): A general framework for computational antibody design. *PLoS computational biology*, 14(4):e1006112, 2018. [1](#), [2](#), [15](#)
- Mansoor Ahmed, Sarwan Ali, Avais Jan, Imdad Ullah Khan, and Murray Patterson. Improved graph-based antibody-aware epitope prediction with protein language model-based embeddings. *bioRxiv*, 2025. doi: 10.1101/2025.02.12.637989. [16](#)
- Sankar Basu and Björn Wallner. Dockq: a quality measure for protein-protein docking models. *PLoS one*, 11(8):e0161879, 2016. [4](#), [10](#)
- Nathaniel R Bennett, Joseph L Watson, Robert J Ragotte, Andrew J Borst, DéJenaé L See, Connor Weidle, Riti Biswas, Yutong Yu, Ellen L Shrock, Russell Ault, et al. Atomically accurate de novo design of antibodies with rfdiffusion. *Nature*, pp. 1–11, 2025. [2](#), [16](#)
- Jiameng Chen, Xiantao Cai, Jia Wu, and Wenbin Hu. Antibody design and optimization with multi-scale equivariant graph diffusion models for accurate complex antigen binding. *arXiv preprint arXiv:2506.20957*, 2025. [5](#), [14](#), [15](#), [18](#)
- Cyrus Chothia and Arthur M Lesk. Canonical structures for the hypervariable regions of immunoglobulins. *Journal of molecular biology*, 196(4):901–917, 1987. [3](#), [13](#)
- Justas Dauparas, Ivan Anishchenko, Nathaniel Bennett, Hua Bai, Robert J Ragotte, Lukas F Milles, Basile IM Wicky, Alexis Courbet, Rob J de Haas, Neville Bethel, et al. Robust deep learning-based protein sequence design using proteinmpnn. *Science*, 378(6615):49–56, 2022. [2](#), [14](#), [16](#)
- James Dunbar and Charlotte M Deane. Anarci: antigen receptor numbering and receptor classification. *Bioinformatics*, 32(2):298–300, 2016. [3](#)
- James Dunbar, Konrad Krawczyk, Jinwoo Leem, Terry Baker, Angelika Fuchs, Guy Georges, Jiye Shi, and Charlotte M Deane. Sabdab: the structural antibody database. *Nucleic acids research*, 42(D1):D1140–D1146, 2014. [1](#), [2](#), [3](#), [15](#)
- Justina Jankauskaitė, Brian Jiménez-García, Justas Dapkūnas, Juan Fernández-Recio, and Iain H Moal. Skempi 2.0: an updated benchmark of changes in protein–protein binding energy, kinetics and thermodynamics upon mutation. *Bioinformatics*, 35(3):462–469, 2019. [2](#), [15](#)
- Wengong Jin, Jeremy Wohlwend, Regina Barzilay, and Tommi Jaakkola. Iterative refinement graph neural network for antibody sequence-structure co-design. *arXiv preprint arXiv:2110.04624*, 2021. [1](#), [2](#), [5](#), [14](#), [18](#)
- Wengong Jin, Regina Barzilay, and Tommi Jaakkola. Antibody-antigen docking and design via hierarchical structure refinement. In *International Conference on Machine Learning*, pp. 10217–10227. PMLR, 2022. [2](#), [5](#), [14](#), [18](#)
- Xiangzhe Kong, Wenbing Huang, and Yang Liu. Conditional antibody design as 3d equivariant graph translation. *arXiv preprint arXiv:2208.06073*, 2022. [1](#), [2](#), [5](#), [14](#), [18](#)
- Xiangzhe Kong, Wenbing Huang, and Yang Liu. End-to-end full-atom antibody design. *arXiv preprint arXiv:2302.00203*, 2023. [1](#), [2](#), [5](#), [14](#), [18](#)
- Marie-Paule Lefranc, Christelle Pommié, Manuel Ruiz, Véronique Giudicelli, Elodie Foulquier, Lisa Truong, Valérie Thouvenin-Contet, and Gérard Lefranc. Imgt unique numbering for immunoglobulin and t cell receptor variable domains and ig superfamily v-like domains. *Developmental & Comparative Immunology*, 27(1):55–77, 2003. [3](#), [13](#)

- Zeming Lin, Halil Akin, Roshan Rao, Brian Hie, Zhongkai Zhu, Wenting Lu, Nikita Smetanin, Robert Verkuil, Ori Kabeli, Yaniv Shmueli, et al. Evolutionary-scale prediction of atomic-level protein structure with a language model. *Science*, 379(6637):1123–1130, 2023. [16](#)
- Chunan Liu, Lilian Denzler, Yihong Chen, Andrew Martin, and Brooks Paige. AsEP: Benchmarking deep learning methods for antibody-specific epitope prediction. *arXiv preprint arXiv:2407.18184*, 2024. [15](#)
- Shitong Luo, Yufeng Su, Xingang Peng, Sheng Wang, Jian Peng, and Jianzhu Ma. Antigen-specific antibody design and optimization with diffusion-based generative models for protein structures. *Advances in Neural Information Processing Systems*, 35:9754–9767, 2022. [1](#), [2](#), [3](#), [5](#), [13](#), [14](#), [18](#)
- Karolis Martinkus, Jan Ludwiczak, Wei-Ching Liang, Julien Lafrance-Vanasse, Isidro Hotzel, Arvind Rajpal, Yan Wu, Kyunghyun Cho, Richard Bonneau, Vladimir Gligorijevic, et al. Ab-diffuser: full-atom generation of in-vitro functioning antibodies. *Advances in Neural Information Processing Systems*, 36:40729–40759, 2023. [1](#)
- Richard Norman, Francesco Ambrosetti, Alexandre Bonvin, Lucy Colwell, Sebastian Kelm, Sandeep Kumar, and Konrad Krawczyk. Computational approaches to therapeutic antibody design: established methods and emerging trends. *Briefings in bioinformatics*, 21(5):1549–1567, 2020. [1](#)
- Pascal Notin, Aaron Kollasch, Daniel Ritter, Lood Van Niekerk, Steffanie Paul, Han Spinner, Nathan Rollins, Ada Shaw, Rose Orenbuch, Ruben Weitzman, et al. Proteingym: Large-scale benchmarks for protein fitness prediction and design. *Advances in Neural Information Processing Systems*, 36:64331–64379, 2023. [2](#), [15](#)
- Thiru Ramaraj, Thomas Angel, Edward A Dratz, Algirdas J Jesaitis, and Suvobrata Bhattacharyya. Antigen–antibody interface properties: Composition, residue interactions, and features of the antigen. *Biochimica et Biophysica Acta (BBA) – Proteins and Proteomics*, 1824(3):520–532, 2012. [11](#)
- Jeffrey A Ruffolo, Lee-Shin Chu, Sai Pooja Mahajan, and Jeffrey J Gray. Fast, accurate antibody structure prediction from deep learning on massive set of natural antibodies. *Nature communications*, 14(1):2389, 2023. [16](#)
- Hannes Stark, Felix Faltings, MinGyu Choi, Yuxin Xie, Eunsu Hur, Timothy O’Donnell, Anton Bushuev, Talip Uçar, Saro Passaro, Weian Mao, et al. Boltzgen: Toward universal binderthe rel design. *bioRxiv*, pp. 2025–11, 2025. [2](#)
- Martin Steinegger and Johannes Söding. Mmseqs2 enables sensitive protein sequence searching for the analysis of massive data sets. *Nature biotechnology*, 35(11):1026–1028, 2017. [3](#), [9](#)
- Cheng Tan, Yijie Zhang, Zhangyang Gao, Yufei Huang, Haitao Lin, Lirong Wu, Fandi Wu, Mathieu Blanchette, and Stan Z Li. dyab: Flow matching for flexible antibody design with alphafold-driven pre-binding antigen. In *Proceedings of the AAAI Conference on Artificial Intelligence*, volume 39, pp. 782–790, 2025. [1](#), [2](#), [5](#), [14](#), [15](#), [18](#)
- Raphael JL Townshend, Martin Vögele, Patricia Suriana, Alexander Derry, Alexander Powers, Yianni Laloudakis, Sidhika Balachandar, Bowen Jing, Brandon Anderson, Stephan Eismann, et al. Atom3d: Tasks on molecules in three dimensions. *arXiv preprint arXiv:2012.04035*, 2020. [2](#)
- Talip Uçar, Cedric Malherbe, and Ferran Gonzalez. Exploring log-likelihood scores for ranking antibody sequence designs. In *NeurIPS 2024 Workshop on AI for New Drug Modalities*, 2024. [14](#)
- Yogesh Verma, Markus Heinonen, and Vikas Garg. Abode: Ab initio antibody design using co-joined odes. In *International Conference on Machine Learning*, pp. 35037–35050. PMLR, 2023. [2](#), [5](#), [14](#), [15](#), [18](#)
- Rubo Wang, Fandi Wu, Jiale Shi, Yidong Song, Yu Kong, Jian Ma, Bing He, Qihong Yan, Tianlei Ying, Peilin Zhao, et al. A generative foundation model for antibody design. *bioRxiv*, pp. 2025–09, 2025. [1](#), [14](#)

- Zichen Wang, Yaokun Ji, Jianing Tian, and Shuangjia Zheng. Retrieval augmented diffusion model for structure-informed antibody design and optimization. *arXiv preprint arXiv:2410.15040*, 2024. [5](#), [14](#), [15](#), [18](#)
- Lirong Wu, Haitao Lin, Yufei Huang, Zhangyang Gao, Cheng Tan, Yunfan Liu, Tailin Wu, and Stan Z Li. Relation-aware equivariant graph networks for epitope-unknown antibody design and specificity optimization. In *Proceedings of the AAAI Conference on Artificial Intelligence*, volume 39, pp. 895–904, 2025. [1](#), [2](#), [5](#), [14](#), [16](#), [18](#)
- Xuezhi Xie, Jin Sub Lee, Dongki Kim, Jaehyeong Jo, Jisun Kim, and Philip M Kim. Antibody-sgm: Antigen-specific joint design of antibody sequence and structure using diffusion models. In *2023 ICML Workshop Comput Biol*, 2023. [14](#)
- Yinghua Yao, Yuangang Pan, and Xixian Chen. Generative co-design of antibody sequences and structures via black-box guidance in a shared latent space. *arXiv preprint arXiv:2508.11424*, 2025. [2](#), [14](#)
- Yang Zhang and Jeffrey Skolnick. Scoring function for automated assessment of protein structure template quality. *Proteins: Structure, Function, and Bioinformatics*, 57(4):702–710, 2004. [4](#), [9](#)
- Xinyan Zhao, Yi-Ching Tang, Akshita Singh, Victor J Cantu, KwanHo An, Junseok Lee, Adam E Stogsdill, Ibraheem M Hamdi, Ashwin Kumar Ramesh, Zhiqiang An, et al. Abbibench: A benchmark for antibody binding affinity maturation and design. *arXiv preprint arXiv:2506.04235*, 2025. [2](#), [15](#)
- Tian Zhu, Milong Ren, and Haicang Zhang. Antibody design using a score-based diffusion model guided by evolutionary, physical and geometric constraints. In *Forty-first International Conference on Machine Learning*, 2024. [2](#), [14](#)
- Yibo Zhu, Xiumin Shi, Jingjuan Zhang, Weizhong Sun, and Lu Wang. Abegdiffuser: Antibody sequence-structure codesign with equivariant graph neural networks and diffusion models. *Journal of Chemical Theory and Computation*, 21(21):11307–11317, 2025. [14](#)

A APPENDIX

A.1 PROCESSING DETAILS

The six sequential quality filters applied during dataset construction are: (1) restriction to protein and peptide antigens, excluding carbohydrates, nucleic acids, and haptens, (2) requirement for both heavy (VH) and light (VL) chains, (3) requirement for an annotated antigen chain, (4) a crystallographic resolution cutoff of 4.0 Å, (5) verification that the structure file was successfully downloaded, and (6) removal of duplicate rows sharing the same PDB, heavy chain, light chain, and antigen chain identifiers. Sequence deduplication concatenates VH and VL sequences for each complex and clusters at 95% identity with 80% coverage using MMseqs2 (Steinegger & Söding, 2017), retaining the highest-resolution representative per cluster, yielding 2,981 deduplicated complexes.

The validation step verifies baseline compatibility by checking four criteria: successful ANARCI numbering for both VH and VL chains, presence of conserved residues at IMGT positions 23 (Cys), 41 (Trp), and 104 (Cys), identifiability of all six CDR regions under IMGT numbering, and no missing C α atoms in any chain. This excludes 59 complexes, of which 27 have missing backbone atoms (mostly peptide antigen termini), 12 contain atypical V-genes that ANARCI cannot number, 11 have engineered conserved-residue substitutions, and 9 have incomplete CDR or conserved-position annotations (including 3 lambda chains lacking CDR-L2 and 6 with missing IMGT anchor positions or CDR regions). The excluded complexes and their reasons are recorded for transparency.

A.2 METRIC DEFINITIONS

We provide formal definitions for all metrics used in CHIMERA-BENCH. Let $\hat{s} = (\hat{s}_1, \dots, \hat{s}_N)$ and $s = (s_1, \dots, s_N)$ denote the predicted and native CDR sequences of length N , $\hat{\mathbf{X}}, \mathbf{X} \in \mathbb{R}^{N \times 3}$ the predicted and native C α coordinates, $m \in \{0, 1\}^N$ the paratope contact mask, and $\mathcal{C}, \hat{\mathcal{C}}$ the native and predicted sets of antibody-antigen contact pairs.

Group 1: Sequence quality.

$$\text{AAR} = \frac{1}{N} \sum_{i=1}^N \mathbb{K}[\hat{s}_i = s_i] \quad (2)$$

$$\text{CAAR} = \frac{\sum_{i=1}^N m_i \cdot \mathbb{K}[\hat{s}_i = s_i]}{\sum_{i=1}^N m_i} \quad (3)$$

$$\text{PPL} = \exp\left(-\frac{1}{N} \sum_{i=1}^N \log p_\theta(s_i \mid \text{context})\right) \quad (4)$$

Group 2: Structural quality. C α RMSD is computed after optimal superposition via SVD-based Kabsch alignment. Let R^* denote the optimal rotation obtained from the SVD of $\hat{\mathbf{X}}_c^\top \mathbf{X}_c$ (centered coordinates):

$$\text{RMSD} = \sqrt{\frac{1}{N} \sum_{i=1}^N \|R^* \hat{\mathbf{x}}_{c,i} - \mathbf{x}_{c,i}\|^2} \quad (5)$$

TM-score (Zhang & Skolnick, 2004) is computed on the Kabsch-aligned structures with length-dependent normalization:

$$\text{TM} = \frac{1}{L} \sum_{i=1}^L \frac{1}{1 + (d_i/d_0)^2}, \quad d_0 = \max(1.24 \sqrt[3]{L} - 1.5, 0.5) \quad (6)$$

where d_i is the distance between aligned C α atoms and L is the target length.

Group 3: Binding interface quality.

$$\text{Fnat} = \frac{|\hat{\mathcal{C}} \cap \mathcal{C}|}{|\mathcal{C}|} \quad (7)$$

$$\text{iRMSD} = \text{RMSD}(\hat{\mathbf{X}}_{\text{iface}}, \mathbf{X}_{\text{iface}}) \quad (8)$$

$$\text{DockQ} = \frac{1}{3} \left(\text{Fnat} + \frac{1}{1 + (\text{iRMSD}/1.5)^2} + \frac{1}{1 + (\text{LRMSD}/8.5)^2} \right) \quad (9)$$

where $\mathbf{X}_{\text{iface}}$ denotes the $C\alpha$ coordinates of interface residues (those participating in contacts) and LRMSD is the Kabsch-aligned $C\alpha$ RMSD of the full antibody (Basu & Wallner, 2016). Native contact sets \mathcal{C} are computed from all heavy-atom coordinates, while predicted contacts $\hat{\mathcal{C}}$ use $C\alpha$ coordinates only (since most generative models produce only backbone atoms).

Group 4: Epitope specificity. Let \hat{E} be the set of antigen residues contacted by the designed antibody (within 4.5 Å) and E the true epitope residues:

$$\text{EpiPrec} = \frac{|\hat{E} \cap E|}{|\hat{E}|}, \quad \text{EpiRec} = \frac{|\hat{E} \cap E|}{|E|}, \quad \text{EpiF1} = \frac{2 \cdot \text{EpiPrec} \cdot \text{EpiRec}}{\text{EpiPrec} + \text{EpiRec}} \quad (10)$$

Group 5: Designability. The sequence liability count is defined as the number of occurrences of known developability liability motifs (NG, DG, DS, DD, NS, NT, M) in the designed CDR sequence.

We further define two evaluation tracks. **Track 1** (CDR-H3 co-design) is mandatory for all methods, since CDR-H3 is the most variable loop and the primary determinant of antigen specificity. **Track 2** (all-CDR co-design) evaluates methods that support multi-loop generation, designing all six CDRs (H1–H3, L1–L3) simultaneously. Few baseline methods natively support epitope conditioning and map directly to the canonical definition. Our epitope-specificity metrics then reveal whether their designs contact the intended binding site.

A.3 DATASET STATISTICS AND ANALYSIS

This section presents the dataset tables, distributional statistics, and figures referenced in the main text. Table 2 summarizes the curation funnel, Table 3 reports structural and interface properties, and Table 4 provides the split sizes.

Table 2: Dataset curation funnel from raw SAbDab to the final CHIMERA-BENCH dataset.

Stage	Complexes
SAbDab summary (all entries)	20,509
After quality filters (resolution, paired chains, antigen type)	9,171
After sequence deduplication (95% identity, 80% coverage)	2,981
After validation (numbering, conserved residues, CDR completeness, backbone)	2,922

Structural properties. Of the 2,922 complexes, 2,485 (85%) target protein antigens and 437 (15%) target peptide antigens. Antigen lengths vary widely (median 196 residues), with longer antigens corresponding to viral surface proteins and shorter ones to peptide epitopes. The dataset is dominated by X-ray diffraction structures (1,929) and cryo-EM structures (989).

Interface properties. Epitope sizes range from 1 to over 50 residues (mean 17.9, median 18), and paratope sizes are slightly larger (mean 20.5, median 20), consistent with the observation that paratope residues span multiple CDR loops while epitope residues cluster on a single antigen surface patch (Figure 3). The mean of 45.6 residue-level contact pairs per complex provides a rich signal for evaluating binding interface reconstruction.

CDR statistics. Under IMGT numbering, CDR-H3 is the most variable loop in both length and sequence (mean 14.6 ± 4.3 residues, range 3–63), with a heavy right tail reflecting the diversity

Table 3: Structural and interface properties of the CHIMERA-BENCH dataset. Values are reported as mean \pm std (median in parentheses where relevant).

Property	Value
Total complexes	2,922
Unique PDBs	2,721
Protein antigens / peptide antigens	2,485 / 437
Resolution (Å)	median 2.72
VH length (IMGT-numbered residues)	121 \pm 5
VL length (IMGT-numbered residues)	108 \pm 3
Full heavy chain length (PDB residues)	189 \pm 44
Full light chain length (PDB residues)	181 \pm 48
Antigen length (PDB residues)	288 \pm 278 (median 196)
Epitope residues per complex	17.9 \pm 8.2 (median 18)
Paratope residues per complex	20.5 \pm 7.1 (median 20)
Contact pairs per complex	45.6 \pm 24.3 (median 44)

Table 4: Summary of CHIMERA-BENCH evaluation splits. All splits use cluster-level assignment to prevent data leakage.

Split	Train	Val	Test	Generalization target
Epitope-group	2,338	292	292	Unseen epitope patterns
Antigen-fold	2,338	292	292	Unseen antigen topologies
Temporal	2,337	292	293	Prospective (post-2023)

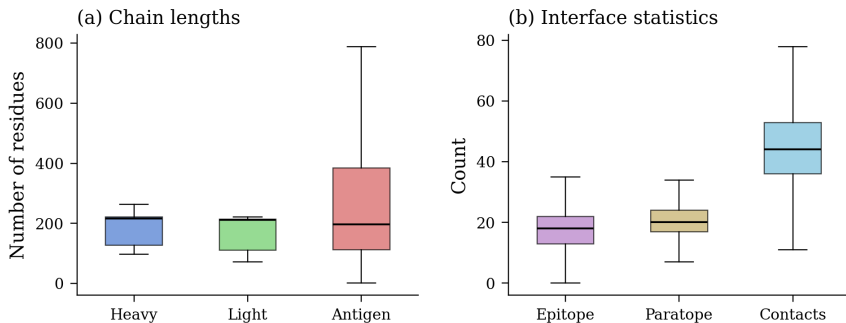


Figure 3: Dataset size distributions. (a) Chain lengths for heavy, light, and antigen chains. (b) Interface statistics: epitope size, paratope size, and number of contact pairs per complex.

of VDJ recombination. CDR-H1 (8.2 ± 0.7) and CDR-H2 (7.9 ± 0.7) show narrower distributions consistent with their more conserved canonical structures. Light chain CDRs are generally more uniform in length: L1 (7.4 ± 2.1), L2 (3.0 ± 0.4 , nearly fixed-length under IMGT), and L3 (9.4 ± 1.3). In our dataset, light-chain residues account for a mean of 35% of paratope contacts (IQR 25–46%), consistent with prior analyses (Ramaraj et al., 2012), and are important for overall interface quality. Full CDR length distributions are shown in Figure 4.

Temporal and species distributions. PDB deposition dates range from the mid-1990s to mid-2024, with a strong concentration in 2019–2023 reflecting the surge in COVID-related antibody structures. The majority of antigens originate from viral proteins or human self-antigens (Figure 5).

Epitope diversity. A distinctive feature of CHIMERA-BENCH is that many antigens are targeted by multiple antibodies binding to distinct epitope regions. Of the 2,470 unique antigen sequences in the dataset, 258 (10.4%) are bound at two or more distinct epitopes, collectively accounting for 710 of the 2,922 complexes (24.3%). The most promiscuous antigen is targeted at 30 distinct epitope sites (Figure 6). This epitope diversity is central to CHIMERA-BENCH’s evaluation, which assesses

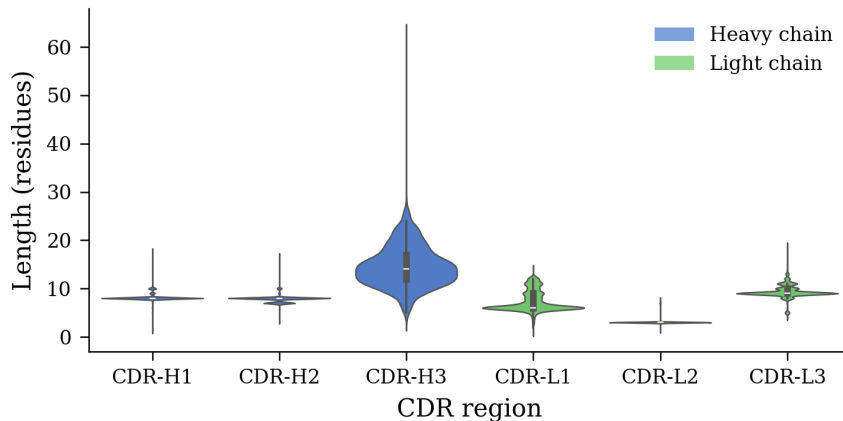


Figure 4: CDR length distributions under IMGT numbering. CDR-H3 shows the widest variability, consistent with its role as the primary determinant of antigen specificity.

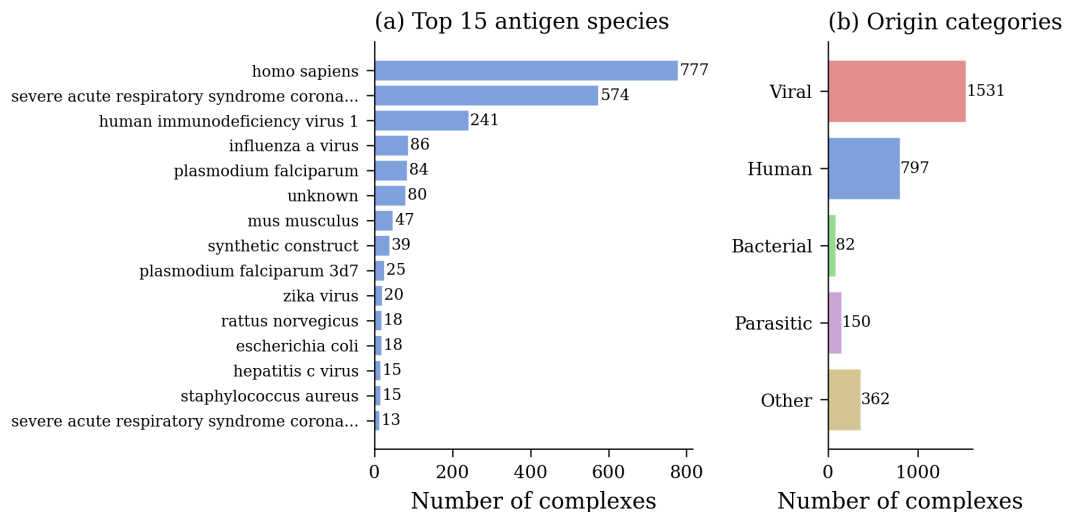


Figure 5: Antigen species and origin distributions. (a) Top 15 species by complex count. (b) Breakdown by biological origin category.

a successful model must not merely reconstruct a plausible binding interface but must do so for the *correct* epitope, making epitope-conditioned generation essential. The epitope-group split explicitly tests this capability by holding out entire epitope clusters at test time.

A.4 PIPELINE CONFIGURATION

Table 5 lists the values of all thresholds and processing parameters used throughout this work. Table 6 provides the CDR boundary definitions under both numbering schemes.

A.5 CROSS-METHOD METRIC COMPARISON

Table 7 summarizes which metrics each of the surveyed methods originally reports, illustrating the inconsistency that CHIMERA-BENCH standardizes. Abbreviations: DP = dynamic-programming RMSD (no Kabsch), K = Kabsch-aligned RMSD, sc = self-consistency RMSD (re-fold then compare), SeqID = BLOSUM62 alignment identity, PLL = pseudo-log-likelihood, LL/NLL = model (negative) log-likelihood.

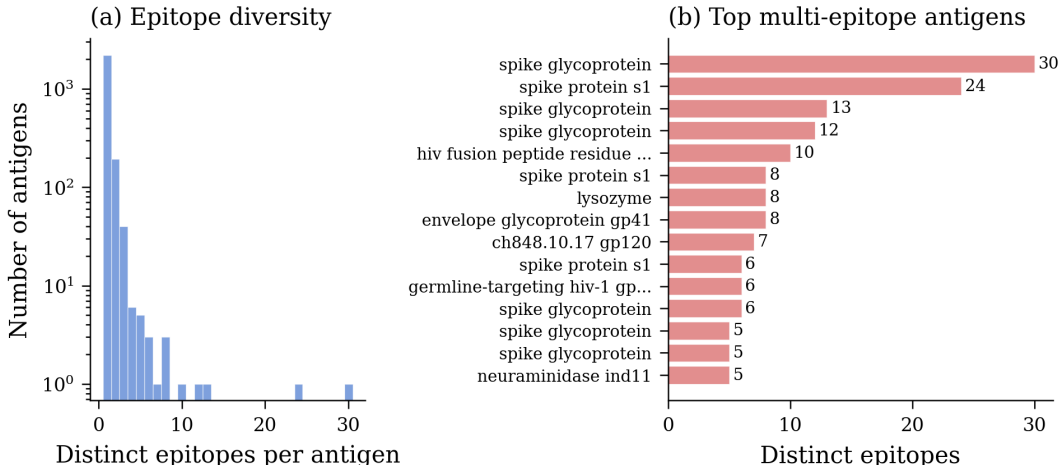


Figure 6: Epitope diversity in CHIMERA-BENCH. (a) Distribution of distinct epitopes per antigen sequence (log scale); most antigens have a single epitope, but a long tail extends to 30. (b) Top 15 multi-epitope antigens ranked by number of distinct epitope sites.

Table 5: Pipeline configuration parameters.

Parameter	Description	Value
Max resolution	Structure quality threshold	4.0 Å
Contact cutoff	Epitope/paratope definition	4.5 Å
Sequence identity	MMseqs2 clustering threshold	95%
Coverage	MMseqs2 alignment coverage	80%
Numbering schemes	Residue numbering	IMGT, Chothia
Graph k -NN	Nearest neighbors for intra-chain edges	10
Graph spatial cutoff	Intra-chain spatial edge threshold	8.0 Å
Inter-chain cutoff	Inter-chain spatial edge threshold	12.0 Å
Train/Val/Test ratio	Split proportions	80/10/10
Temporal split	Date-based quantile cutoffs	80/10/10

Table 6: CDR boundary definitions used in CHIMERA-BENCH.

Scheme	H1	H2	H3	L1	L2	L3
IMGT (Lefranc et al., 2003)	27–38	56–65	105–117	27–38	56–65	105–117
Chothia (Chothia & Lesk, 1987)	26–32	52–56	95–102	24–34	50–56	89–97

A.6 BASELINE RETRAINING ON CHIMERA-BENCH

All baselines are retrained on CHIMERA-BENCH using the authors’ released code with default hyperparameters. We provide a shared training and evaluation framework that handles data loading in each method’s native input format, split-aware partitioning, early stopping, model checkpointing, and performs full evaluation. Each complex is identified by a composite key consisting of the PDB code and its heavy, light, and antigen chain identifiers, which resolves the ambiguity that arises when multiple complexes share the same PDB file with different chain assignments. At test time, per-complex predictions are evaluated against native structures using all metrics defined in Section 3.4. All training and inference is performed on an NVIDIA A100 GPU. Below we describe the method-specific adaptations required for each baseline.

DiffAb. DiffAb (Luo et al., 2022) operates under the Chothia numbering scheme and generates all six CDRs simultaneously by randomly masking between one and six CDRs during training. At inference, all CDRs are masked and regenerated in a single forward pass, producing one set of predictions per complex from which per-CDR metrics are extracted. We train with Adam at a

Table 7: Metrics originally reported by each method (prior to CHIMERA-BENCH standardization).

Method	AAR	RMSD	TM	IDDT	DockQ	PPL	dG/IMP	CAAR
MEAN (Kong et al., 2022)	AAR	K	✓	–	–	✓	ddG	–
dyMEAN (Kong et al., 2023)	AAR	K	✓	✓	✓	–	ddG	✓
RAAD (Wu et al., 2025)	AAR	K	✓	–	–	✓	–	–
RefineGNN (Jin et al., 2021)	AAR	K	–	–	–	✓	–	–
AbODE (Verma et al., 2023)	AAR	K	–	–	–	✓	–	–
AbDockGen (Jin et al., 2022)	AAR	K	–	–	✓	✓	–	–
DiffAb (Luo et al., 2022)	SeqID	DP	–	–	–	–	IMP,dG	–
dyAb (Tan et al., 2025)	AAR	K	✓	✓	✓	–	ddG	✓
RADAb (Wang et al., 2024)	AAR	sc	–	–	–	PLL	ddG	–
AbFlowNet (Abir et al., 2025)	SeqID	DP	–	–	–	–	IMP,dG	–
AbX (Zhu et al., 2024)	AAR	K	–	–	–	PLL	IMP	–
AbEgDiffuser (Zhu et al., 2025)	AAR	DP	–	–	–	–	IMP	–
AbMEGD (Chen et al., 2025)	SeqID	DP	–	–	–	–	IMP	–
AbSGM (Xie et al., 2023)	–	K	–	–	–	–	–	–
LEAD (Yao et al., 2025)	AAR	DP	–	–	–	–	ddG	–
ProteinMPNN (Dauparas et al., 2022)	AAR	–	–	–	–	NLL	–	–
IgGM (Wang et al., 2025)	AAR	K	✓	✓	✓	–	–	–
DiffAbXL (Uçar et al., 2024)	–	–	–	–	–	LL	–	–

learning rate of 10^{-4} and a batch size of 16, using 100 diffusion steps with equal loss weights on rotation, position, and sequence terms.

RAAD. RAAD (Wu et al., 2025) generates one CDR at a time, requiring three training runs per split. We use the Adam optimizer with a learning rate of 10^{-3} and a batch size of 8. The model employs four relation-aware equivariant message-passing layers and constructs multi-relational graphs with radial, k -nearest neighbor, sequential, and global edge types. The structure loss weight is set to $\alpha=0.8$, placing greater emphasis on coordinate accuracy compared to MEAN.

MEAN. Because MEAN (Kong et al., 2022) generates a single CDR loop per forward pass, we train three separate models per split to cover H1, H2, and H3. Each model is optimized with Adam at a learning rate of 10^{-3} and a batch size of 16. The structure loss is weighted by $\alpha=0.05$ relative to the sequence loss, and the model performs five multi-channel equivariant attention iterations per forward pass to progressively refine the generated CDR.

dyMEAN. dyMEAN (Kong et al., 2023) supports flexible CDR selection and performs three iterative refinement rounds per forward pass. The learning rate decays exponentially from 10^{-3} to 10^{-4} with a batch size of 4. A cosine annealing schedule linearly decreases the fraction of native template information provided to the model, gradually forcing reliance on its own predictions. The paratope is defined using a 6.6 Å contact threshold under IMGT numbering.

RefineGNN. RefineGNN (Jin et al., 2021) generates CDR residues autoregressively from left to right while iteratively refining the predicted backbone structure after each residue is placed. Like MEAN and RAAD, it generates one CDR per forward pass, so we train three separate models per split for H1, H2, and H3. The model uses four message-passing layers with a hidden dimension of 256 and constructs k -nearest-neighbor graphs with $k=9$. A bidirectional GRU encodes framework context, and the structural refinement step runs at every position (update frequency 1), predicting pairwise distances that are converted to coordinates via eigendecomposition. During training, teacher forcing provides the ground-truth sequence at each step, while at inference, the model samples from the predicted distribution autoregressively.

AbDockGen. AbDockGen (Jin et al., 2022) is a hierarchical equivariant refinement network that generates CDR-H3 conditioned on the epitope surface, making it applicable only to **Track 1** evaluation. The model encodes the top 20 nearest epitope residues using an E(3)-equivariant graph neural network and generates the CDR-H3 sequence and structure autoregressively with iterative coordinate refinement. The architecture consists of four hierarchical EGNN layers with a hidden di-

mension of 256 and $k=9$ nearest neighbors, operating at both atom and residue levels. Explicit clash avoidance constraints enforce minimum distances of 3.8 Å between backbone atoms and 1.5 Å between side-chain atoms during coordinate updates. We train with Adam at a learning rate of 10^{-3} , dynamic batching at 100 tokens, and gradient clipping at norm 1.0, for at most 10 epochs with a learning rate anneal factor of 0.9.

AbODE. AbODE (Verma et al., 2023) formulates CDR generation as a conjoined ordinary differential equation that jointly evolves sequence logits and backbone coordinates. Like MEAN and RAAD, it generates one CDR at a time and requires three training runs per split. The model consists of four TransformerConv layers and we train with Adam at a learning rate of 10^{-3} and a batch size of 1 due to variable-size fully-connected graphs.

AbFlowNet. AbFlowNet (Abir et al., 2025) extends DiffAb’s diffusion architecture with a GFlowNet trajectory balance objective to optimize binding energy. It uses Chothia numbering and generates all six CDRs simultaneously. The training-time backward loss is disabled for CHIMERA integration. We train with Adam at a learning rate of 10^{-4} and a batch size of 16.

AbMEGD. AbMEGD (Chen et al., 2025) is a multi-CDR diffusion model that shares DiffAb’s Chothia-based preprocessing pipeline and generates all six CDRs simultaneously. We train with the authors’ default hyperparameters using Adam optimization.

RADAb. RADAb (Wang et al., 2024) is a retrieval-augmented diffusion model that combines DiffAb’s diffusion framework with sequence retrieval from a FASTA database. It uses ESM-2 (650M parameters) for sequence embeddings and an MSA transformer for retrieved sequence alignment. We train under Chothia numbering with Adam optimization.

dyAb. dyAb (Tan et al., 2025) applies flow matching to flexible antibody design under IMGT numbering, generating all six CDRs simultaneously. The model includes OpenMM-based structure relaxation and a DDG prediction module. We train with the authors’ default configuration.

A.7 COMPARISON WITH PRIOR BENCHMARKS

Table 8 compares CHIMERA-BENCH with prior benchmarks (RAbD (Adolf-Bryfogle et al., 2018), SAbDab (Dunbar et al., 2014), SKEMPI v2 (Jankauskaitė et al., 2019), AsEP (Liu et al., 2024), AbBiBench (Zhao et al., 2025), ProteinGym (Notin et al., 2023)) used for developing and evaluating antibody and protein design methods. CHIMERA-BENCH is the largest curated benchmark of its kind and the first to combine standardized epitope annotations, multiple evaluation splits, and cross-method format compatibility.

Table 8: Comparison of CHIMERA-BENCH with prior antibody design benchmarks and datasets.

	CHIMERA-BENCH	RAbD	SAbDab	SKEMPI v2	AsEP	AbBiBench	ProteinGym
Domain	Ab design	Ab design	Ab structures	Affinity	Epitope pred.	Affinity mat.	Fitness
Complexes	2,922	60	7,000+	53 (Ab)	1,723	14 Ab / 9 Ag	–
Epitope labels	✓	–	–	–	✓	–	–
Paratope labels	✓	–	–	–	✓	–	–
CDR annotations	✓	–	–	–	–	–	–
Multiple splits	3	1	–	1	2	3	3
Leakage prevention	✓	–	–	–	✓	✓	✓
Baselines evaluated	11	1	–	–	5	15	70+
Affinity data	–	–	Partial	✓	–	✓	✓

A.8 LIMITATIONS.

CHIMERA-BENCH evaluates designs against static crystallographic structures and does not account for conformational flexibility or solvent effects. The dataset inherits the biases of SAbDab and the PDB more broadly: co-crystal structures are dominated by viral surface proteins (particularly from the COVID-era surge in SARS-CoV-2 antibody structures deposited 2020–2023), human-derived antibodies, and X-ray crystallography (66% of complexes). Antigens from bacterial, fungal, or

parasitic pathogens are underrepresented, as are camelid and synthetic antibody formats. CDR-H3 lengths follow a heavy-tailed distribution (mean 14.6, 95th percentile 22 residues) with rare extreme outliers (only 0.03% exceed 35 residues), reflecting the natural diversity of VDJ recombination rather than data artifacts. RFAntibody (Bennett et al., 2025) can perform CDR redesign in principle, but its weights are trained on the full PDB without a disclosed split, and no retraining code is available, making leakage-controlled evaluation infeasible under CHIMERA-BENCH’s protocol. Inverse folding (fixed-backbone sequence design) is an important complementary task that CHIMERA-BENCH can support through Track 1 evaluation; benchmarking methods such as ProteinMPNN (Dauparas et al., 2022) in this setting is planned as future work.

A.9 RESIDUE GRAPH CONSTRUCTION

For each complex, we construct a heterogeneous multi-relational residue graph (Wu et al., 2025) stored as a PyG `HeteroData` object. The graph contains three node types corresponding to heavy chain, light chain, and antigen residues.

Node features (105D). Each residue node carries a 105-dimensional feature vector consisting of a residue type one-hot encoding (20D), sinusoidal positional encoding along the chain (16D), backbone dihedral angle sin/cos encodings (12D for 6 angles), radial basis function (RBF) encodings of $C\alpha$ -to-backbone-atom distances (48D for 3 atoms with 16 RBF bins each), and a local coordinate frame derived from N, $C\alpha$, C atoms via Gram–Schmidt orthogonalization (9D). Each node additionally stores the residue type index, backbone atom coordinates (N, $C\alpha$, C, O), CDR region labels under IMGT numbering, a binary flag marking designable CDR positions, and binary epitope or paratope labels. Since pre-trained protein language model (PLM) embeddings are proven to capture meaningful evolutionary features of proteins (Ahmed et al., 2025), we utilize ESM2 (Lin et al., 2023) to compute embeddings for antigens and AntiBERTy (Ruffolo et al., 2023) for antibodies.

Intra-chain edges. Within each chain, four relation types encode complementary structural relationships. Sequential ± 1 edges connect adjacent residues along the backbone, sequential ± 2 edges provide broader backbone context, k -nearest neighbor edges ($k=10$) capture local 3D proximity regardless of sequence position, and spatial edges connect all residue pairs within 8.0 Å not already covered by the preceding types. Each intra-chain edge carries a 39-dimensional feature vector consisting of edge type one-hot (4D), relative positional encoding (16D), $C\alpha$ - $C\alpha$ distance RBF encoding (16D), and normalized direction vector (3D).

Inter-chain edges. Two types of inter-chain edges connect antibody and antigen nodes. Contact edges are derived from the annotated contact pairs (4.5 Å heavy-atom cutoff) and directly encode the binding interface by linking heavy-to-antigen and light-to-antigen residue pairs. Spatial edges use a broader 12 Å $C\alpha$ - $C\alpha$ cutoff with 16-bin RBF distance features, providing the spatial context used by MEAN, dyMEAN, dyAb, and RAAD for message passing across chains. Heavy-to-light spatial edges are also included for intra-antibody context.

The resulting graphs are saved as a single dictionary mapping complex identifiers to `HeteroData` objects. These precomputed graphs can be used directly by graph-based methods or converted to homogeneous representations as needed.

A.10 QUALITATIVE CDR-H3 STRUCTURE COMPARISON

Figure 7 shows the predicted CDR-H3 backbone structures from seven methods overlaid on the native loop for three complexes selected to illustrate different design regimes.

7JKS (H3 length 14) is a typical case where equivariant GNN methods (RAAD, dyMEAN) recover the native sequence well (AAR \sim 0.36) with moderate RMSD (\sim 1.6 Å), while diffusion-based methods achieve lower AAR (\sim 0.17–0.33) with slightly higher RMSD (\sim 2.1–2.7 Å). AbODE produces the lowest RMSD (0.61 Å) but with lower sequence recovery (AAR=0.29), consistent with the paradigm-level trends observed in the main results.

4J4P (H3 length 17) represents a case where equivariant GNNs and diffusion methods disagree. dyMEAN achieves the highest AAR (0.71) while diffusion methods recover substantially fewer

residues (AAR \sim 0.13–0.27). RMSD values diverge widely, from 1.50 Å (AbODE) to 5.44 Å (dyAb), illustrating how longer loops amplify structural prediction errors.

4XMP (H3 length 25) is a challenging long-loop case where all methods struggle. AAR drops below 0.18 for every method, and RMSD ranges from 1.52 Å (AbODE) to 11.64 Å (DiffAb). The diffusion-based methods produce particularly large deviations on this long loop, while AbODE again achieves low CDR RMSD despite poor sequence recovery, reinforcing the disconnect between local loop quality and sequence accuracy.

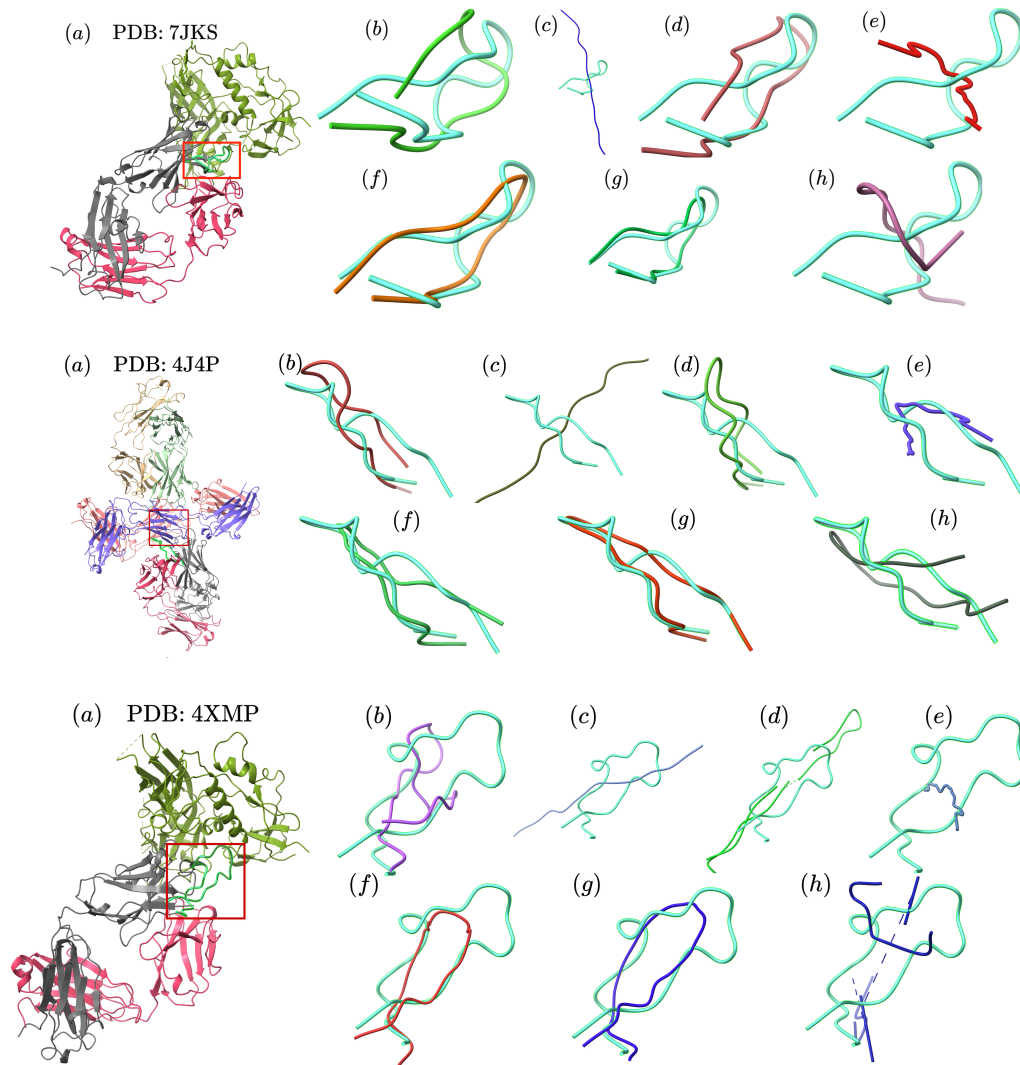


Figure 7: Native (a) and predicted CDR-H3 backbone structures for three complexes of increasing difficulty: 7JKS (H3 length 14), 4J4P (H3 length 17), and 4XMP (H3 length 25). Panels show predictions from (b) AbFlowNet, (c) AbODE, (d) DiffAb, (e) dyAb, (f) dyMEAN, (g) RAAD, (h) RefineGNN. The native CDR H3 regions are shown in cyan colors.

A.11 ADDITIONAL RESULTS

Tables 9 and 10 report CDR-H3 co-design results on the antigen-fold and temporal test splits, respectively. These complement the epitope-group results in Table 1. Table 11 presents all-CDR results (Track 2) for the six multi-CDR baselines on the epitope-group split, revealing a clear CDR difficulty hierarchy: H3 is hardest (lowest AAR, highest RMSD), while L2 and H1 are easiest.

Table 9: CDR-H3 design results on the **antigen-fold** test split.

Method	AAR \uparrow	CAAR \uparrow	PPL \downarrow	RMSD \downarrow	TM \uparrow	Fnat \uparrow	iRMSD \downarrow	DockQ \uparrow	EpiF1 \uparrow	n.liab. \downarrow
RAAD (Wu et al., 2025)	0.38\pm0.13	0.24 \pm 0.24	3.32 \pm 0.50	1.71 \pm 0.72	0.23 \pm 0.12	0.03 \pm 0.04	0.94 \pm 0.51	0.58 \pm 0.07	0.11 \pm 0.15	0.52 \pm 0.61
MEAN (Kong et al., 2022)	0.37 \pm 0.13	0.24 \pm 0.23	3.28 \pm 0.60	1.79 \pm 0.75	0.20 \pm 0.10	0.03 \pm 0.04	1.02 \pm 0.56	0.57 \pm 0.07	0.13 \pm 0.16	0.78 \pm 0.42
dyMEAN (Kong et al., 2023)	0.38\pm0.13	0.25\pm0.24	3.26\pm0.47	2.09 \pm 0.89	0.17 \pm 0.10	0.04 \pm 0.05	1.31 \pm 0.78	0.55 \pm 0.08	0.16 \pm 0.19	0.93 \pm 0.25
DiffAb (Luo et al., 2022)	0.24 \pm 0.13	0.15 \pm 0.19	–	3.60 \pm 22.88	0.16 \pm 0.15	0.04 \pm 0.05	1.72 \pm 1.20	0.50 \pm 0.13	0.22\pm0.21	0.46\pm0.71
AbFlowNet (Abir et al., 2025)	0.24 \pm 0.12	0.16 \pm 0.19	–	2.21 \pm 1.09	0.17 \pm 0.16	0.04 \pm 0.05	1.47 \pm 0.84	0.51 \pm 0.13	0.20 \pm 0.21	0.87 \pm 1.04
AbMEGD (Chen et al., 2025)	0.22 \pm 0.13	0.14 \pm 0.18	–	2.55 \pm 3.44	0.16 \pm 0.15	0.05\pm0.06	1.62 \pm 2.37	0.51 \pm 0.13	0.22\pm0.21	0.58 \pm 0.79
RADAb (Wang et al., 2024)	0.17 \pm 0.12	0.10 \pm 0.17	–	2.31 \pm 1.11	0.15 \pm 0.14	0.04 \pm 0.04	1.50 \pm 0.78	0.51 \pm 0.13	0.19 \pm 0.18	0.59 \pm 0.80
dyAb (Tan et al., 2025)	0.25 \pm 0.10	0.15 \pm 0.19	–	2.31 \pm 1.11	0.13 \pm 0.10	0.03 \pm 0.04	1.55 \pm 0.67	0.51 \pm 0.07	0.12 \pm 0.16	1.88 \pm 0.40
RefineGNN (Jin et al., 2021)	0.21 \pm 0.13	0.10 \pm 0.15	9.24 \pm 4.26	2.58 \pm 0.62	0.11 \pm 0.08	0.03 \pm 0.04	0.90\pm0.45	0.59\pm0.06	0.14 \pm 0.16	0.53 \pm 0.72
AbDockGen (Jin et al., 2022)	0.23 \pm 0.11	0.11 \pm 0.16	7.15 \pm 2.35	4.07 \pm 1.27	0.04 \pm 0.02	0.03 \pm 0.06	3.84 \pm 2.01	0.37 \pm 0.09	0.14 \pm 0.15	0.57 \pm 0.68
AbODE (Verma et al., 2023)	0.36 \pm 0.13	0.22 \pm 0.22	9.49 \pm 5.48	1.06\pm0.40	0.32\pm0.14	0.02 \pm 0.03	10.33 \pm 5.23	0.25 \pm 0.09	0.07 \pm 0.12	0.47 \pm 0.58

Table 10: CDR-H3 design results on the **temporal** test split.

Method	AAR \uparrow	CAAR \uparrow	PPL \downarrow	RMSD \downarrow	TM \uparrow	Fnat \uparrow	iRMSD \downarrow	DockQ \uparrow	EpiF1 \uparrow	n.liab. \downarrow
RAAD (Wu et al., 2025)	0.38\pm0.13	0.22 \pm 0.22	3.26 \pm 0.44	1.78 \pm 0.74	0.22 \pm 0.11	0.03 \pm 0.05	1.02 \pm 0.56	0.58\pm0.06	0.12 \pm 0.13	0.68 \pm 0.59
MEAN (Kong et al., 2022)	0.38\pm0.13	0.23\pm0.22	3.23\pm0.43	1.87 \pm 0.66	0.17 \pm 0.07	0.03 \pm 0.04	1.04 \pm 0.55	0.57 \pm 0.06	0.09 \pm 0.11	0.56 \pm 0.67
dyMEAN (Kong et al., 2023)	0.37 \pm 0.13	0.22 \pm 0.22	3.41 \pm 0.48	2.26 \pm 0.90	0.15 \pm 0.09	0.03 \pm 0.04	1.36 \pm 0.75	0.54 \pm 0.08	0.10 \pm 0.13	0.62 \pm 0.48
DiffAb (Luo et al., 2022)	0.24 \pm 0.11	0.14 \pm 0.16	–	2.45 \pm 1.04	0.13 \pm 0.11	0.04 \pm 0.05	1.63 \pm 0.81	0.50 \pm 0.11	0.20\pm0.17	0.25 \pm 0.50
AbFlowNet (Abir et al., 2025)	0.22 \pm 0.10	0.13 \pm 0.16	–	4.61 \pm 25.83	0.12 \pm 0.11	0.05\pm0.05	2.06 \pm 3.94	0.49 \pm 0.12	0.20\pm0.17	0.58 \pm 0.78
AbMEGD (Chen et al., 2025)	0.23 \pm 0.11	0.14 \pm 0.18	–	2.59 \pm 1.12	0.12 \pm 0.10	0.04 \pm 0.05	1.75 \pm 0.79	0.49 \pm 0.11	0.17 \pm 0.16	0.48 \pm 0.68
RADAb (Wang et al., 2024)	0.20 \pm 0.11	0.10 \pm 0.15	–	4.39 \pm 28.15	0.10 \pm 0.07	0.04 \pm 0.05	2.69 \pm 16.09	0.49 \pm 0.11	0.19 \pm 0.17	1.38 \pm 1.30
dyAb (Tan et al., 2025)	0.23 \pm 0.09	0.12 \pm 0.18	–	2.46 \pm 0.99	0.11 \pm 0.07	0.02 \pm 0.03	1.68 \pm 0.71	0.50 \pm 0.06	0.08 \pm 0.11	0.94 \pm 0.23
RefineGNN (Jin et al., 2021)	0.21 \pm 0.12	0.10 \pm 0.16	9.23 \pm 3.67	2.72 \pm 0.61	0.09 \pm 0.05	0.03 \pm 0.05	0.97\pm0.51	0.58\pm0.06	0.12 \pm 0.14	0.64 \pm 0.73
AbDockGen (Jin et al., 2022)	0.23 \pm 0.11	0.10 \pm 0.16	8.78 \pm 2.99	4.63 \pm 1.22	0.03 \pm 0.02	0.02 \pm 0.03	3.72 \pm 1.78	0.37 \pm 0.08	0.10 \pm 0.11	0.60 \pm 0.82
AbODE (Verma et al., 2023)	0.35 \pm 0.13	0.20 \pm 0.21	9.82 \pm 4.12	1.09\pm0.38	0.31\pm0.12	0.02 \pm 0.03	11.63 \pm 5.43	0.21 \pm 0.08	0.06 \pm 0.10	0.24\pm0.46

Table 11: Per-CDR results on the **epitope-group** test split. Mean AAR, RMSD, and EpiF1 are shown per CDR type. “–” indicates the method does not support the given CDR. Best values are in **bold**, second-best are underlined.

Method	AAR \uparrow						RMSD \downarrow						EpiF1 \uparrow					
	H1	H2	H3	L1	L2	L3	H1	H2	H3	L1	L2	L3	H1	H2	H3	L1	L2	L3
RAAD	0.71	0.63	0.37	–	–	–	0.54	0.50	1.75	–	–	–	0.09	0.09	0.11	–	–	–
MEAN	0.67	0.57	0.37	–	–	–	0.91	0.84	1.84	–	–	–	0.08	0.09	0.10	–	–	–
dyMEAN	0.62	0.60	0.37	–	–	–	1.20	0.89	2.22	–	–	–	0.10	0.11	0.23	–	–	–
DiffAb	0.57	0.30	0.23	0.57	0.48	0.42	0.75	0.84	2.49	1.03	0.49	0.91	0.09	0.09	0.20	0.10	0.09	0.10
AbFlowNet	0.59	0.31	0.23	0.56	0.49	0.40	0.77	0.66	2.38	1.05	0.50	0.95	0.10	0.09	0.20	0.10	0.09	0.12
AbMEGD	0.54	0.32	0.21	0.45	0.43	0.35	0.82	0.73	2.44	1.29	0.64	1.00	0.09	0.09	0.20	0.10	0.09	0.10
RADAb	0.54	0.28	0.20	0.45	0.43	0.36	0.94	0.86	5.33	1.42	4.20	1.16	0.08	0.09	0.17	0.10	0.09	0.11
dyAb	0.34	0.23	0.19	0.34	0.31	0.33	1.04	1.17	2.34	1.51	0.52	1.09	0.09	0.09	0.11	0.10	0.09	0.11
RefineGNN	0.54	0.44	0.21	–	–	–	2.61	1.90	2.86	–	–	–	0.09	0.09	0.15	–	–	–
AbDockGen	–	–	0.24	–	–	–	–	–	4.67	–	–	–	–	–	0.08	–	–	–
AbODE	0.54	0.47	0.26	–	–	–	0.48	0.39	1.07	–	–	–	0.09	0.11	0.07	–	–	–